

# Green's Function Formalism for Waveguide QED Applications

Michael P. Schneider,<sup>1,\*</sup> Tobias Sproll,<sup>1,\*</sup> Christina Stawiarski,<sup>2</sup> Peter Schmitteckert,<sup>2,3</sup> and Kurt Busch<sup>1,4</sup>

<sup>1</sup>*Max-Born-Institut, Max-Born-Str. 2A, 12489 Berlin, Germany*

<sup>2</sup>*Institut für Theorie der Kondensierten Materie and DFG-Center for Functional Nanostructures, Karlsruher Institut für Technologie, 76128 Karlsruhe, Germany*

<sup>3</sup>*Institut für Nanotechnologie, Karlsruher Institut für Technologie, 76021 Karlsruhe, Germany*

<sup>4</sup>*Humboldt-Universität zu Berlin, Institut für Physik, AG Theoretische Optik & Photonik, Newtonstr. 15, 12489 Berlin*

We present a quantum-field-theoretical framework based on path integrals and Feynman diagrams for the investigation of the quantum-optical properties of one-dimensional waveguiding structures with embedded quantum impurities. In particular, we obtain the Green's functions for a waveguide with an embedded two-level system in the single- and two-excitation sector for arbitrary dispersion relations both in the time and the frequency domain. In the single excitation sector, we show how to sum the diagrammatic perturbation series to all orders and thus obtain explicit expressions for physical quantities such as the spectral density and the scattering matrix. In the two-excitation sector, we show that strictly linear dispersion relations exhibit the special property that the corresponding diagrammatic perturbation series terminates after two terms, again allowing for closed-form expressions for physical quantities. In the case of general dispersion relations, notably those exhibiting a band edge or waveguide cut-off frequencies, the perturbation series cannot be summed explicitly. Instead, we derive a self-consistent  $T$ -matrix equation that reduces the computational effort to that of a single-excitation computation. This analysis allows us to identify a Fano resonance between the occupied quantum impurity and a free photon in the waveguide as a unique signature of the few-photon nonlinearity inherent in such systems. In addition, our diagrammatic approach allows for the classification of different physical processes such as the creation of photon-photon correlations and interaction-induced radiation trapping – the latter being absent for strictly linear dispersion relations. Our framework can serve as the basis for further studies that involve more complex scenarios such as several and many-level quantum impurities, networks of coupled waveguides, disordered systems, and non-equilibrium effects.

## I. INTRODUCTION

Presently, research on nano-scale quantum-optical (NQO) systems is witnessing an increasing amount of attention worldwide and several distinct experimental approaches have been developed to a point where the realization of complex functional elements becomes feasible. Besides ordinary integrated optical waveguides and Photonic Crystals with embedded quantum impurities [1–3] these systems also include superconducting waveguide-QED settings [4, 5] and fiber systems with nearby trapped atoms [6]. In view of the fact that efficient integrated single-photon sources [7–10] and advanced integrated single-photon detectors [11–14] are available, the design and control of few-photon nonlinearities moves more and more into the focus of research efforts [15, 16]. Such integrated sources, integrated detectors, and controlled few-photon nonlinearities represent the basic building blocks for future integrated quantum information processing technologies [17].

From a theoretical angle, the transport of few photons in waveguiding systems and their interaction with quantum impurities exhibits certain similarities with nano-electronic transport problems so that several methodologies of electron transport theory have been adapted

to the analysis of NQO systems. These include (i) a Bethe-Ansatz approach [18], the Lehmann-Symanzik-Zimmermann reduction technique [19] and the Input-Output formalism [20] for determining the multi-particle scattering matrix and (ii) a Green's function approach has been developed that exploits the chirality of effective low-energy field theories which are derived from the basic Hamiltonian (see Eqs. (1) and (2) below) [21]. These approaches have also been extended to the case of many photons [22, 23] and more complicated quantum impurities [24]. Furthermore, direct numerical approaches have been developed [25–27] some of them going beyond the rotating wave approximation that is implied with the aforementioned basic Hamiltonian [28].

In the present work, we develop a versatile quantum-field-theoretical framework for the analysis of NQO systems that consist of combinations of photonic waveguiding elements with embedded quantum impurities. Our framework is based on a path-integral formulation and the construction of associated Feynman diagrams. This facilitates the formulation of an efficient Green's function technique. We demonstrate the efficiency of our framework by rederiving the main results of the above-mentioned approaches and extending them to arbitrary dispersion relations, notably for the case of two photons. In addition, our approach provides novel and detailed insights into the physical processes that underlie photon correlations effects and the existence of bound photon-atom states in such systems.

---

\*These two authors contributed equally

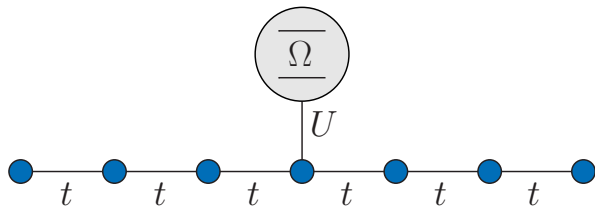


FIG. 1: Graphic representation of the model considered in this work: A tight-binding bosonic chain with interchain hopping  $t$  (representing a photonic waveguide) is site-coupled to a fermionic two-level system with level spacing  $\Omega$  and the few-photon transport through this system is studied.

The manuscript is organized as follows. In Sec. II, we describe the basic physical model and provide the corresponding path-integral formulation in Sec. III. This leads to a representation in Feynman diagrams which we elaborate on in Sec. IV. As Green's function are the central element of any diagrammatic approach, we discuss their properties in the single- and two-excitation sectors in Secs. V and VI, respectively. The results are summarized in Sec. VII and several technical aspects are relegated to appendices.

## II. THE MODEL

We consider a one-dimensional bosonic quantum wire formed by a chain of sites to which a (fermionic) two-level system (TLS) is side-coupled, as sketched in Fig. 1. The corresponding Hamiltonian is given by

$$H = -t \sum_x \left( a_x^\dagger a_{x+1} + \text{h.c.} \right) + \frac{\Omega}{2} \sigma_z + U \left( a_0^\dagger \sigma_- + \text{h.c.} \right), \quad (1)$$

where  $a_x^\dagger$  is a bosonic creation operator at site  $x$ ,  $t$  is the in-chain hopping constant between nearest-neighbor sites of the wire. The TLS is described by the level spacing  $\Omega$  and the corresponding Pauli matrix  $\sigma_z$ . The coupling (with strength  $U$ ) between the quantum wire and the TLS is facilitated by the product of the TLS lowering operator  $\sigma_-$  and the photon creation operator  $a_x^\dagger$ . Further, h.c. denotes hermitian conjugation and all lengths have been scaled by the lattice spacing  $a$ . This prototypical Hamiltonian thus describes the propagation of photons in a waveguide that interact with an embedded quantum impurity, the TLS, within the rotating wave approximation. At this point, we would like to note that the above bosonic sites could be regarded as identical physical resonators that are coupled through overlapping field distributions. Such systems have been fabricated in coupled-resonator [29], photonic crystal- [30] and fiber-optical [31] settings and their cosine-type dispersion relation has indeed been observed. Alternatively (and more generally), these bosonic sites could be regarded as the

numerical discretization of an arbitrary waveguide with a given dispersion relation. This dispersion relation can be modeled by going beyond the nearest-neighbor hopping in the bosonic chain. However, typical waveguide dispersion relations usually feature (i) slow-light regimes in the vicinity of band edges or waveguide cut-off frequencies and/or (ii) frequency ranges with an almost linear dispersion relation. The tight-binding model, too, exhibits these features for frequencies near the edges and in the middle of the band, respectively, so that this model may serve as a good approximation for specific frequency ranges of general dispersion relations.

Upon spatially Fourier-transforming Eq. (1), we obtain

$$H = \sum_k \epsilon(k) a_k^\dagger a_k + \frac{\Omega}{2} \sigma_z + \frac{U}{\sqrt{L}} \sum_k \left( a_k^\dagger \sigma_- + \text{h.c.} \right), \quad (2)$$

where  $L$  is the system size and  $\epsilon(k) = -2t \cos(k)$  is the dispersion relation of the tight-binding chain. Note that the above Hamiltonian conserves the excitation number

$$N = \sum_k a_k^\dagger a_k + \frac{1}{2} (\sigma_z + 1), \quad (3)$$

which means that the Hilbert space factorizes into subspaces of constant excitation number (as a matter of fact, we will only consider the cases  $N = 1$  and  $N = 2$  here). As a last step, we replace the Pauli spin operators by auxiliary fermions,

$$\sigma_z = f^\dagger f - g^\dagger g \quad (4)$$

$$\sigma_- = g^\dagger f, \quad (5)$$

which requires that the constraint

$$f^\dagger f + g^\dagger g = 1, \quad (6)$$

has to be fulfilled. Here,  $f^\dagger$  and  $g^\dagger$  are, respectively, the creation operators of the excited and ground state of the TLS. Hence, the Hamiltonian which we use for the remainder of this work is

$$H = \sum_k \epsilon(k) a_k^\dagger a_k + \frac{\Omega}{2} (f^\dagger f - g^\dagger g) + \frac{U}{\sqrt{L}} \sum_k \left( a_k^\dagger g^\dagger f + \text{h.c.} \right). \quad (7)$$

The Hamiltonian (1) exhibits strong similarities to well-known models in quantum optics and condensed-matter theory. Specifically, the Hamiltonian could either be seen as a spin-boson model, a multi-mode generalization of the Jaynes-Cummings model [32], a Dicke model [33], or a spinless, partly bosonic version of the Anderson impurity model [34] without on-site interaction. As discussed above, this invites the adaptation of tools that have been developed for the analyses of these models, albeit bearing in mind the different physics and the resulting different questions that shall be addressed. In fact,

path-integral and related Green's function techniques are among the most flexible approaches, allowing for closed-form solutions in simple cases and providing efficient perturbative approaches for challenging cases such as disordered systems[35] and systems out of equilibrium[36].

### III. PATH INTEGRAL APPROACH

We begin our exposition by defining the Green's function as the matrix element of an initial and a final state at different times

$$G(t_f - t_i) = -i \langle f | e^{-\int_{t_i}^{t_f} H(t) dt} | i \rangle, \quad (8)$$

where  $H$  is a generic Hamiltonian. In addition,  $|i\rangle$  and  $|f\rangle$  represent, respectively, the initial and the final state. For a path-integral representation, we utilize the resolution of unity via coherent states

$$\mathbb{1} = \frac{1}{(2\pi i)^c} \int \prod_{\alpha} d\psi_{\alpha} d\psi_{\alpha}^* e^{-\sum_{\alpha} \psi_{\alpha}^* \psi_{\alpha}} |\psi_{\alpha}\rangle \langle \psi_{\alpha}|, \quad (9)$$

where  $c = 1$  for complex fields,  $c = 0$  for Grassman fields, and  $\alpha$  labels the set of associated one-particle states ( $|\psi_{\alpha}\rangle \langle \psi_{\alpha}|$  being the corresponding projection operator). Inserting this resolution of unity twice into Eq. (8) yields

$$G(t_f - t_i) = -i \int \prod_{m,n} d\psi_{i,m} d\psi_{i,m}^* d\psi_{f,n} d\psi_{f,n}^* e^{-\sum_m \psi_{i,m}^* \psi_{i,m} - \sum_n \psi_{f,n}^* \psi_{f,n}} \langle f | \psi_f \rangle \langle \psi_i | i \rangle G(f, i; t_f - t_i). \quad (10)$$

Here  $G(f, i, t_f - t_i)$  is given by

$$G(f, i; t_f - t_i) = \langle \psi_f | e^{-\int_{t_i}^{t_f} H(t) dt} | \psi_i \rangle, \quad (11)$$

so that the labels  $i$  and  $f$  represent the initial and final fields,  $\psi_i$  and  $\psi_f$ , respectively. In the above equations, the indices  $m$  and  $n$  run over the number of different modes that occur in the generic Hamiltonian  $H$  by virtue of corresponding creation and annihilation operators.

In the case of the Hamiltonian given by Eq. (7), we have to introduce three types fields: Complex fields  $\phi_k$  for the bosonic modes in the waveguide and two Grassmann fields  $\theta$  and  $\chi$ , which correspond to the fermionic operators  $f$  and  $g$ , respectively. With these definitions, Eq. (10) reads

$$G(t_f - t_i) = -i \int \prod_{k,k'} d\phi_{i,k} d\phi_{i,k}^* d\phi_{f,k'} d\phi_{f,k'}^* e^{-\sum_k \phi_{i,k}^* \phi_{i,k} - \sum_k \phi_{f,k}^* \phi_{f,k}} \langle \text{ph}_f | \phi_f \rangle \langle \phi_i | \text{ph}_i \rangle G(f, i; t_f - t_i), \quad (12)$$

where we have absorbed the integration over the Grassman fields into

$$G(f, i; t_f - t_i) = \int d\chi_i d\chi_i^* d\chi_f d\chi_f^* d\theta_i d\theta_i^* d\theta_f d\theta_f^* e^{-\chi_i^* \chi_i - \chi_f^* \chi_f - \theta_i^* \theta_i - \theta_f^* \theta_f} \times \langle \text{TLS}_f | \chi_f \theta_f \rangle \langle \chi_i \theta_i | \text{TLS}_i \rangle \langle \phi_f \chi_f \theta_f | e^{-\int_{t_i}^{t_f} H(t) dt} | \phi_i \chi_i \theta_i \rangle. \quad (13)$$

In the above equations, we have employed a decomposition of the system's initial state into a product of a part for the photons with a part for the two-level system

$$|i\rangle = |\text{ph}_i\rangle \otimes |\text{TLS}_i\rangle. \quad (14)$$

In addition, we have employed an analogous decomposition for the final state.

For the calculation of  $G(f, i, t_f - t_i)$  we mainly follow the lines of Ref. 37, so that we will restrict ourselves to the relevant intermediate steps. Upon inserting the resolution of unity  $N$  times in Eq. (13), we arrive at

$$G(f, i; t_f - t_i) = \int d\chi_i d\chi_i^* d\chi_f d\chi_f^* d\theta_i d\theta_i^* d\theta_f d\theta_f^* e^{-\chi_i^* \chi_i - \chi_f^* \chi_f - \theta_i^* \theta_i - \theta_f^* \theta_f} \langle \text{TLS}_f | \chi_f \theta_f \rangle \langle \chi_i \theta_i | \text{TLS}_i \rangle \times \lim_{N \rightarrow \infty} \int \prod_{m=1}^N \prod_{n=1}^{N-1} \prod_k \frac{d\phi_{n,k} d\phi_{n,k}^* d\theta_n d\theta_n^* d\chi_n d\chi_n^*}{2\pi i} \times e^{-\sum_{n,k} (\phi_{n,k} \phi_{n,k}^* + \chi_n \chi_n^* + \theta_n \theta_n^*)} e^{-i\eta H(\phi_m, \phi_{m-1}^*, \chi_m, \chi_{m-1}^*, \theta_m, \theta_{m-1}^*)}, \quad (15)$$

where  $\eta = \frac{t_f - t_i}{N}$  and

$$H(\phi_n, \phi_{n-1}^*, \chi_n, \chi_{n-1}^*, \theta_n, \theta_{n-1}^*) = \sum_k \epsilon(k) \phi_{n,k} \phi_{n-1,k}^* + \frac{\Omega}{2} (\theta_n \theta_{n-1}^* - \chi_n \chi_{n-1}^*) + \frac{U}{\sqrt{N}} \sum_k (\phi_{n,k}^* \chi_n^* \theta_{n-1} + \theta_n^* \chi_{n-1} \phi_{n-1,k}). \quad (16)$$

The labels  $n = 0$  and  $n = N$  correspond, respectively, to the initial and final fields. Next, we integrate out the intermediate fermionic degrees of freedom and obtain

$$G(f, i; t_f - t_i) = \int d\chi_i d\chi_i^* d\chi_f d\chi_f^* d\theta_i d\theta_i^* d\theta_f d\theta_f^* e^{-\chi_i^* \chi_i - \chi_f^* \chi_f - \theta_i^* \theta_i - \theta_f^* \theta_f} \langle \text{TLS}_f | \chi_f \theta_f \rangle \langle \chi_i \theta_i | \text{TLS}_i \rangle \\ \times \lim_{N \rightarrow \infty} \int \prod_{n=1}^{N-1} \prod_k \frac{d\phi_{n,k} d\phi_{n,k}^*}{2\pi i} e^{-\sum_{n,k} \phi_{n,k} \phi_{n,k}^* (1 - i\eta \epsilon(k))} e^{\vec{q}_N^\dagger R(\phi, \phi^*) \vec{q}_0}. \quad (17)$$

Here, we have introduced the following abbreviations

$$q_i = (\theta_i, \chi_i), \quad R(\phi, \phi^*) = R(\phi_N, \phi_{N-1}^*) \cdot \dots \cdot R(\phi_1, \phi_0^*),$$

$$R(\phi_i, \phi_{i-1}^*) = \begin{pmatrix} 1 - i\eta\Omega/2 & 0 \\ 0 & 1 + i\eta\Omega/2 \end{pmatrix} - i\eta \frac{U}{\sqrt{L}} \sum_k \begin{pmatrix} 0 & \phi_{i-1,k} \\ \phi_{i,k}^* & 0 \end{pmatrix}. \quad (18)$$

The TLS can either be in the excited or in the ground state. Thus, we can write the TLS' state as a vector

$$|\text{TLS}\rangle = \begin{pmatrix} |e\rangle \\ |g\rangle \end{pmatrix}, \quad (19)$$

which induces a matrix structure to  $G(f, i; t_f - t_i)$

$$G(f, i; t_f - t_i) = \begin{pmatrix} G_e(f, i; t_f - t_i) & G_{ab}(f, i; t_f - t_i) \\ G_{em}(f, i; t_f - t_i) & G_w(f, i; t_f - t_i) \end{pmatrix}. \quad (20)$$

The nomenclature of this matrix notation is as follows. We denote the case when the TLS is excited in the initial as well as in the final state by the diagonal element  $G_e$ . Consequently,  $G_e$  covers the dynamics of the quantum impurity, i.e., the TLS that interacts with photons from the waveguide so that we call it the TLS-Green's function. Similarly, we denote the case when the TLS is in the ground state for both the initial and the final state by the diagonal element  $G_w$ . Clearly, this quantity describes the dynamics of the photons in the waveguide in the presence of the TLS and we, therefore, call it the waveguide Green's function. The off-diagonal element  $G_{ab}$  features that the TLS is initially in the ground state, but ends up being in the excited state. This means that the TLS has absorbed a photon, hence we call  $G_{ab}$  the absorption Green's function. Clearly,  $G_{em}$  covers the complementary process and we call it the emission Green's function.

We now utilize the fermionic resolution of unity and the identities [37]  $\langle e | \theta \chi \rangle = \theta$ ,  $\langle g | \theta \chi \rangle = \chi$ , and  $\theta \chi^* = e^{-\theta \chi^*} - 1$  to perform the last integration over the fermionic fields. We will restrict ourselves to the TLS-Green's function, the other Green's functions can be determined in exactly the same way. Following the procedure in Ref. 37, we find

$$G_e(f, i, t_f - t_i) = \lim_{N \rightarrow \infty} \int \prod_{n=1}^{N-1} \prod_k \frac{d\phi_{k,n} d\phi_{k,n}^*}{2\pi i} e^{-\sum_{n,k} \phi_{n,k} \phi_{n,k}^* (1 - i\eta \epsilon(k))} R(\phi, \phi^*). \quad (21)$$

In the next step, we want to integrate out the bosonic fields. Therefore, we use the matrix  $R(\phi, \phi^*)$  (see Eq. (18))

and expand it up to  $\mathcal{O}(\eta)$ . Taking the limit  $N \rightarrow \infty$  at the end, we find

$$\begin{aligned}
G_e(f, i; t_f - t_i) &= \sum_{r=0}^{\infty} \left( \frac{iU}{\sqrt{L}} \right)^r \int_0^{t_i - t_f} dt_{2r} \int_0^{t_{2r}} dt_{2r-1} \dots \int_0^{t_2} dt_1 \prod_k \prod_{m=1}^{2r} \frac{d\phi_{m,k} d\phi_{m,k}^*}{2\pi i} \\
&\times G_{e,0}(\phi_N^*, \phi_{2r}, t_f - t_i - t_{2r}) e^{-\sum_k \phi_{2r,k}^* \phi_{2r,k}} \sum_k \phi_{2r,k} \\
&\times G_{w,0}(\phi_{2r}^*, \phi_{2r-1}, t_{2r} - t_{2r-1}) e^{-\sum_k \phi_{2r-1,k}^* \phi_{2r-1,k}} \sum_k \phi_{2r-1,k}^* \\
&\times G_{e,0}(\phi_{2r-1}^*, \phi_{2r-2}, t_{2r-1} - t_{2r-2}) e^{-\sum_k \phi_{2r-2,k}^* \phi_{2r-2,k}} \sum_k \phi_{2r-2,k} \\
&\dots \\
&\times G_{e,0}(\phi_1^*, \phi_0, t_1).
\end{aligned} \tag{22}$$

Here, we have introduced the free propagators of the excited TLS and the waveguide

$$G_{e/w,0}(\phi_i^*, \phi_j, t) = e^{\mp i \frac{\Omega}{2} t} e^{\sum_k \phi_{i,k}^* e^{-i\epsilon(k)t} \phi_{j,k}}. \tag{23}$$

Further, we would like to note that at this point the correspondence to an ordinary perturbation series becomes clear. We have vertices with strength  $\frac{U}{\sqrt{L}}$  at which a photon is annihilated or created and the free propagation of photons or excitations between two successive scattering events.

In order to calculate the full Green's function, we have to evaluate Eq. (12). For an  $n$ -photon state, the projection on the coherent states is given by

$$\langle k_1 k_2 \dots k_n | \phi \rangle = \phi_{k_1} \phi_{k_2} \dots \phi_{k_n}. \tag{24}$$

Inserting these bosonic fields and integrating out the bosonic variables finally yields the full Green's functions. As our basic (and equivalent) Hamiltonians, Eqs. (1) and (2), conserve the total number of excitations (cf. Eq. (3)), we proceed by evaluating the TLS-Green's function explicitly for the single- and two-excitation sectors.

### A. Single excitation sector

For a single excitation, we start the evaluation of the TLS-Green's function  ${}_1G_e(t_f - t_i)$  by noting that we have an initial and final state where the TLS is excited and there are no photons in the waveguide. The TLS-Green's function then reads

$${}_1G_e(t_f - t_i) = -i \int \prod_{k,k'} d\phi_{f,k} d\phi_{f,k}^* d\phi_{i,k'} d\phi_{i,k'}^* e^{-\sum_k \phi_{f,k} \phi_{f,k}^* - \sum_k \phi_{i,k} \phi_{i,k}^*} G_e(f, i, t_f - t_i). \tag{25}$$

The dependence on the fields  $\phi_f, \phi_i$  is easily integrated out and we obtain

$$\begin{aligned}
{}_1G_e(t_f - t_i) &= -i \sum_{r=0}^{\infty} \left( \frac{iU}{\sqrt{L}} \right)^{2r} \int_0^{t_i - t_f} dt_{2r} \int_0^{t_{2r}} dt_{2r-1} \dots \int_0^{t_2} dt_1 \\
&\times G_e^0(t_f - t_i - t_{2r}) G_w^{0,\Sigma}(t_{2r} - t_{2r-1}) G_e^0(t_{2r-1} - t_{2r-2}) \dots G_e^0(t_1 - t_0) \\
&= \sum_r {}_1G_e^{(r)}(t_f - t_i)
\end{aligned} \tag{26}$$

We note that every term of the sum has the form of a Dyson series and represents a convolution  ${}_1G_e^{(r)} \sim \underbrace{G_e^0 * G_w^{0,\Sigma} * G_e^0 \dots * G_e^0}_{2r+1 \text{ factors}}$  with

$${}_1G_e^0(t) = e^{-i \frac{\Omega}{2} t}, \quad {}_1G_w^{0,\Sigma}(t) = e^{i \frac{\Omega}{2} t} \sum_k e^{-i\epsilon(k)t} = \sum_k {}_1G_w^0(k, t). \tag{27}$$

By means of the convolution theorem, we can recast this in Fourier space as an algebraic equation

$${}_1G_e(\omega) = \sum_{r=0}^{\infty} \frac{1}{\omega - \Omega/2 + i\delta} \left( \frac{1}{\omega - \Omega/2 + i\delta} \sum_k \frac{U^2/L}{\omega + (\Omega/2 - \epsilon(k)) + i\delta} \right)^r. \quad (28)$$

Here, we have introduced the factors  $+i\delta$  because we are working with retarded Green's functions, i.e., the limit  $\delta \rightarrow 0+$  should be understood.

The above equation can readily be solved, and we arrive at the main equation of this section, the TLS-Green's function  ${}_1G_e(\omega)$  in the single-excitation sector

$${}_1G_e(\omega) = \frac{1}{\omega - \Omega/2 + i\delta - {}_1\Sigma(\omega)}, \quad (29)$$

where the self-energy  ${}_1\Sigma(\omega)$  is given by

$${}_1\Sigma(\omega) = \frac{U^2}{L} \sum_k \frac{1}{\omega + \Omega/2 - \epsilon(k) + i\delta}. \quad (30)$$

The waveguide-Green's function in the single excitation sector can be calculated in a similar manner as the above TLS-Green's function. The main difference lies in the fact that the initial and final states feature a free photon. As a result, one has to add free photon fields in Eq. (25), which yields

$${}_1G_w(k_i, k_f; t_f - t_i) = -i \int \prod_{k, k'} d\phi_{f, k} d\phi_{f, k}^* d\phi_{i, k'} d\phi_{i, k'}^* \phi_{i, k_i}^* \phi_{f, k_f} e^{-\sum_k \phi_{f, k} \phi_{f, k}^* - \sum_k \phi_{i, k} \phi_{i, k}^*} G_w(f, i; t_f - t_i). \quad (31)$$

Performing the integrations and again transiting to momentum space results in

$${}_1G_w(k_i, k_f; \omega) = {}_1G_w^0(k_i; \omega) \delta_{k_i, k_f} + \frac{U^2}{L} {}_1G_w^0(k_i; \omega) {}_1G_e(\omega) {}_1G_w^0(k_f; \omega), \quad (32)$$

where

$${}_1G_w^0(k; \omega) = \frac{1}{\omega + \Omega/2 - \epsilon(k) + i\delta}. \quad (33)$$

The expression (32) for the waveguide-Green's function  ${}_1G_w(k_i, k_f; \omega)$  consists two terms, which can be identified with free propagation of the photon and scattering off the (renormalized) TLS, respectively. The corresponding absorption and emission Green's functions are derived in Appendix A, together with their diagrammatic representation.

## B. Two excitation sector

In this sub-section, we consider two excitations in our system. Again, we start with determining the Green's function for an excited impurity in the initial and in the final state, i.e., the TLS-Green's function  ${}_2G_e$ . The starting point is the general expression given by Eq. (12). As compared with the single-excitation case, the only difference is that, according to Eq. (24), we now have an additional bosonic excitation in the in- and out state. Consequently, for this specific case  $G(t_f - t_i)$  reads

$${}_2G_e(k_i, k_f; t_f - t_i) = -i \int \prod_{k, k'} d\phi_{f, k} d\phi_{f, k}^* d\phi_{i, k'} d\phi_{i, k'}^* \phi_{i, k_i}^* \phi_{f, k_f} e^{-\sum_k \phi_{f, k} \phi_{f, k}^* - \sum_k \phi_{i, k} \phi_{i, k}^*} G_e(f, i, t_f - t_i), \quad (34)$$

where  $G_e(f, i, t_f - t_i)$  is given by (22). Integration over the bosonic degrees of freedom is performed along the same lines as in the previous sub-section. Again transiting to momentum space, the Green's function is given by

$$\begin{aligned} {}_2G_e(k_f, k_i; \omega) = & {}_2G_{e,r}(k_i; \omega) \delta_{k_i, k_f} \\ & + \frac{U^2}{L} {}_2G_{e,r}(k_i; \omega) {}_2G_w^0(k_f, k_i; \omega) {}_2G_{e,r}(k_f; \omega) \\ & + \frac{U^4}{L^2} \sum_k {}_2G_{e,r}(k_i; \omega) {}_2G_w^0(k_i, k; \omega) {}_2G_{e,r}(k; \omega) {}_2G_w^0(k, k_f; \omega) {}_2G_{e,r}(k_f; \omega) \\ & + \dots, \end{aligned} \quad (35)$$

where

$${}_2G_w^0(k, k'; \omega) = \frac{1}{\omega + \Omega/2 - \epsilon(k) - \epsilon(k') + i\delta} \quad (36)$$

and

$${}_2G_{e,r}(k; \omega) = \frac{1}{\omega - \Omega/2 - \epsilon(k) + i\delta - {}_2\Sigma(k; \omega)}. \quad (37)$$

The self-energy  ${}_2\Sigma(k; \omega)$  is given by

$${}_2\Sigma(k; \omega) = \frac{U^2}{L} \sum_{k'} {}_2G_w^0(k, k'; \omega). \quad (38)$$

While we cannot express  ${}_2G_e(k_f, k_i; \omega)$  in closed form, we can recast Eq. (35) in a T-Matrix representation which can easily be accessed numerically. Explicitly, the T-Matrix representation reads

$${}_2G_e(k_f, k_i; \omega) = {}_2G_{e,r}(k_i; \omega) \delta_{k_i, k_f} + {}_2G_{e,r}(k_i; \omega) T(k_f, k_i; \omega) {}_2G_{e,r}(k_f; \omega) \quad (39)$$

with the T-matrix

$$T(k_f, k_i; \omega) = \frac{U^2}{L} {}_2G_w^0(k_f, k_i; \omega) + \frac{U^2}{L} \sum_k {}_2G_w^0(k, k_i; \omega) {}_2G_{e,r}(k; \omega) T(k_f, k; \omega). \quad (40)$$

The above T-matrix representation of  ${}_2G_e(k_f, k_i; \omega)$ , Eqs. (39) and (40), constitutes one of the main results of our work. Eq. (39) describes the nontrivial behavior of the TLS in the presence of an additional photon. Clearly, the result is more complicated than in the single-excitation case, where we were able to solve a standard Dyson equation. In the present case of two excitations, however, we have found a self-consistent description of the Green's function, which can be solved numerically for arbitrary dispersion relations. Furthermore, in the special case of a linear dispersion relation, the TLS-Green's function can even be calculated analytically (see section VI B).

The corresponding waveguide-Green's function, which describes the behavior of two photons in the presence of an impurity in the ground state is given by

$$\begin{aligned} {}_2G_w(k_i, p_i, k_f, p_f; t_f - t_i) = & -i \int \prod_{k, k'} d\phi_{f,k} d\phi_{f,k}^* d\phi_{i,k'} d\phi_{i,k'}^* \\ & \times \phi_{i,k_i}^* \phi_{i,p_i}^* \phi_{f,k_f} \phi_{f,p_f} e^{-\sum_k \phi_{f,k} \phi_{f,k}^* - \sum_k \phi_{i,k} \phi_{i,k}^*} G_w(f, i, t_f - t_i). \end{aligned} \quad (41)$$

After performing the integrations, the waveguide-Green's function finally reads

$$\begin{aligned} {}_2G_w(\omega, k_f, p_f, k_i, p_i) = & {}_2G_w^0(k_i, p_i; \omega) (\delta_{k_i, k_f} \delta_{p_i, p_f} + \delta_{k_i, p_f} \delta_{p_i, k_f}) \\ & + \frac{U^2}{L} {}_2G_w^0(\omega, k_i, p_i) {}_2G_e^{\text{sym}}(k_i, p_i, k_f, p_f; \omega) {}_2G_w^0(\omega, k_f, p_f), \end{aligned} \quad (42)$$

where  ${}_2G_e^{\text{sym}}$  is a symmetrized version of the full TLS-Green's function and is given by

$${}_2G_e^{\text{sym}}(k_i, p_i, k_f, p_f; \omega) = {}_2G_e(k_f, k_i; \omega) + {}_2G_e(k_f, p_i; \omega) + {}_2G_e(p_f, k_i; \omega) + {}_2G_e(p_f, p_i; \omega). \quad (43)$$

For the case of two excitations, the full waveguide-Green's function  ${}_2G_w(\omega, k_f, p_f, k_i, p_i)$  exhibits the same structure as in the single-excitation sector. It consists of a free propagation term and a second term that describes the scattering off a renormalized TLS. For the absorption and emission Green's functions, we provide the expressions for the two-excitation sector in Appendix B along with their diagrammatic representation.

#### IV. FEYNMAN DIAGRAM REPRESENTATION

In this section, we illustrate the formulas obtained by the path integral approach by way of Feynman diagrams. Specifically, we will refrain from providing a rigorous derivation of the full diagrammatic technique but will instead represent the equations of the previous section by Feynman diagrams. This "visualization" provides a clear identification and interpretation of physical pro-

cesses and, as already alluded to above, facilitates a very flexible and efficient framework for perturbative analyses.

In general, the Hamiltonian given by Eq. (7) features three distinct species of quantized excitations, i.e., bosons (photons) with a mode index  $k$  and two types of fermions, representing the excited and the ground state of the TLS. In the following diagrammatic representation, these excitations will be depicted by a wavy, a dashed and a solid line, respectively. This mapping is also shown in Tab. I for clarification. Apart from these diagonal contributions, Eq. (7) also features a scattering vertex, which connects the individual lines and is also shown in Tab. I.

As much of the physical insight to be gained originates from a comparison of the results for the case of a single excitations with the case of two excitations, we will proceed in a corresponding sequence of sub-sections.

### A. Single excitation sector

In the case of a single excitation our first goal is to depict the TLS-Green's function  ${}_1G_e$  in terms of Feynman diagrams. Upon inspecting Eq. (26) we find two distinct contributions. The first contribution stems from

$${}_1G_e^0(t' - t) = e^{-i\frac{\Omega}{2}(t' - t)} = \text{---} \rightarrow \text{---} \quad (44)$$

and describes the propagation of an excited TLS from time  $t$  to  $t'$ . The second contribution is given by (cf. Eq. (27))

$${}_1G_w^0(k, t' - t) = e^{i\frac{\Omega}{2}(t' - t)} e^{-i\epsilon(k)(t' - t)} = \begin{array}{c} \text{~~~~~} \\ \text{-----} \end{array}, \quad (45)$$

and describes the simultaneous transport of a TLS in the ground state together with a photon in the waveguide from time  $t$  to  $t'$ . Furthermore, we can infer from Eq. (26) that each vertex is weighted by a factor  $iU/\sqrt{L}$ . Combining everything we can rewrite the TLS-Green's function diagrammatically as


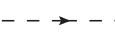

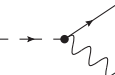
Photons	$ e\rangle$	$ g\rangle$	Vertex
			

TABLE I: Table of the representation of the individual species and the interaction vertex in terms of Feynman diagrams.

$${}_1G_e(t_f - t_i) = -i \left\{ \begin{array}{l} \text{---} \rightarrow \text{---} \\ + \text{---} \rightarrow \text{---} \text{---} \text{---} \text{---} \\ + \text{---} \rightarrow \text{---} \text{---} \text{---} \text{---} \text{---} \\ + \dots \end{array} \right\} \quad (46)$$

where each vertex provides an integration over internal times. Additionally, each photonic line sandwiched between two interaction vertices implies a summation over the corresponding momentum. At this point we are able to exploit one of the main advantages of the diagrammatic approach and provide an interpretation of the individual terms in the perturbation series in terms of physical processes: The excited TLS goes to the ground state by emitting a photon. This photon is absorbed at a later time, setting the TLS to the excited state again. This process is repeated  $n$  times in the  $n$ th term of the perturbation series.

In the frequency domain, the convolution integrals associated with the time-domain diagrams turn into simple products, so that we may retain the free propagation and the bubble diagram as well as the entire perturbation series. Therefore, in the frequency domain no integration with regards to the scattering vertices are implied and per bubble only a weighting factor of  $U/\sqrt{L}$  is implied, furthermore the global prefactor  $-i$  can be omitted. However, each sandwiched photonic line still comes with a summation over the corresponding momentum. Explicitly, the free TLS-Green's function reads

$$\text{---} \rightarrow \text{---} = \frac{1}{\omega - \Omega/2 + i\delta} = {}_1G_e^0(\omega). \quad (47)$$

Similarly, in the frequency domain, we evaluate the bubble diagram after cutting it free from the interaction vertices to

$$\begin{array}{c} \text{~~~~~} \\ \text{-----} \end{array} = \frac{1}{\omega + \Omega/2 - \epsilon(k) + i\delta} = {}_1G_w^0(k; \omega). \quad (48)$$

In the time-domain this Green's function describes the simultaneous propagation of a TLS in the ground state and a photon in the waveguide. Since both excitations are created and annihilated at the same times, the Fourier transform yields only one frequency argument and leads to the analytic form shown above.

As usual, we can cast the perturbation series (46) into the form of a self-consistent Dyson equation

$${}_1G_e(\omega) = \text{---} \text{---} (\Sigma) \text{---} \text{---} \\ = \text{---} \text{---} + \text{---} \text{---} \text{---} \text{---} (\Sigma) \text{---} \text{---}, \quad (49)$$



which can be readily solved and we obtain Eq. (29) with the self-energy

$${}_1\Sigma(\omega) = \frac{U^2}{L} \sum_k {}_1G_w^0(k; \omega) = \text{bubble diagram} \quad (50)$$

By the same token, the full waveguide-Green's function is given by Eq. (32) and we can represent it in a diagrammatic form

$${}_1G_w(k_f, k_i; \omega) = \text{free propagation} + \text{scattering off TLS} \quad (51)$$

This expression comprises two terms. The first term on r.h.s. corresponds to the free propagation of a photon and the TLS in the ground state while the second term on the r.h.s. describes the scattering off the (renormalized) TLS. Upon reinserting Eq. (46) into Eq. (51), we obtain the perturbation series of the full waveguide-Green's function. At this point, we would like to note that the full waveguide-Green's function still carries only one frequency, which is a manifestation of the fact that both, the photon and the ground state propagation, start and end at the same time.

### B. Two excitation sector

We now turn to the case where we have an additional photon in the system, i.e., we want to develop the diagrammatic description of Sec. III B. From Eq. (35) we know that the perturbation series for the TLS-Green's function consists of two Green's functions, which we will depict diagrammatically as

$${}_2G_w^0(k, k'; t_f - t_i) = \text{two free photons} \quad (52)$$

and

$${}_2G_{e,r}(k; t_f - t_i) = \text{excited TLS} \quad (53)$$

Just as in the single-excitation case, these Green's functions describe the propagation of the excitations over a given time interval from  $t_i$  to  $t_f$  (this behavior can be immediately understood by the single frequency dependence in Eq. (36) and (37)). The Green's function  ${}_2G_w^0(k, k'; t_f - t_i)$  describes the simultaneous propagation of two photons with momenta  $k$  and  $k'$ , together with a ground state field of the TLS. Similarly, the Green's function  ${}_2G_{e,r}(k; t_f - t_i)$  represents the propagation of

an excited TLS and one additional photon. In addition, in Eq. (53) we have already encapsulated bubble-like renormalizations into the excited TLS propagation (as discussed in the single-excitation case).

With the help of these basic Green's function, we can now rewrite the TLS-Green's function in the two-excitation case as given by Eq. (35) within the Feynman diagrammatic formulation as

$${}_2G_e(k, k', t_f - t_i) = -i \left\{ \begin{array}{l} \text{self-energy bubble} \\ \text{one interaction} \\ \text{two interactions} \\ \dots \end{array} \right\} \quad (54)$$

Here, the dotted lines serves as indicator that separate distinct Green's functions from each other and - in the time-domain formulation - imply an integration over the associated intermediate times. Furthermore, the momentum of the free photon is conserved (as long as it does not interact with a vertex), each interaction vertex provides a factor  $iU/\sqrt{L}$  and photons sandwiched between two interaction vertices imply a summation over the corresponding momentum (this applies for the upper, sandwiched photon in the third term, for example). For the interested reader, we have layed down the way to the equal-time Green's functions in Appendix C.

This diagrammatic formulation of the TLS-Green's function's perturbation series in the two-excitation case provides a clear physical interpretation. The first term of the perturbation series corresponds to the situation when the TLS is excited and the additional photon is and stays free throughout the entire propagation. In the second term, the excited TLS emits a photon at some intermediate time, so for a given period of time two photons exist in the waveguide and propagate freely along with a free propagation of the TLS in the ground state. After a certain time the initially free photon is absorbed by the TLS, whereas the other photon continues to propagate freely. Clearly, this induces correlations between the photons. In the higher-order terms of the perturbation series this process is repeated many times, which effectively leads to photons that are emitted and reabsorbed, while the respective other photon is scattered by the TLS. Finally, we would like to note that all processes where the TLS directly reabsorbs the originally emitted photon without intermediate scattering are contained in the self-energy bubbles. In the case of a frequency-domain description, the intermediate convolutions integrals translate into multiplications and the common time-dependencies of the individual free-particle propagators that comprise the TLS-Green's function lead

to a single frequency argument, just as has been the case for the single-excitation case.

The full waveguide-Green's function is given by Eq. (42) and can be obtained by adding free waveguide-Green's functions to the full TLS-Green's function  ${}_2G_e(k, k', \omega)$  in a symmetrized way (see Eq. (42)) and by augmenting the perturbation series by a further term that takes into account the free propagation as described by Eq. (52).

A general and very important property of the system is that the TLS cannot interact with free photons if it is in the excited state. It is exactly this property which renders the system nonlinear, so that it is interesting to see how this feature translates into the diagrammatic formalism. For a linear system (e.g., a one-dimensional waveguide with a site-coupled bosonic quantum dot instead of the TLS) with two excitations, we could just take the square of the single excitation propagator, which, in our model, would lead to double excitations of the bosonic quantum dot. As already noted, the two-excitation Green's functions which we use have only one time dependence, so that the particles (photons (bosons) and the two fermions corresponding to the TLS in the ground and excited state, respectively) are created and annihilated at the same times. This means that the second term on the r.h.s. of Eq. (54) can be interpreted as follows. A photon and an excited TLS are created at time  $t_i$  and propagate up to an intermediate time  $\tau$ . At this time, the TLS emits an additional photon and goes to the ground state, until at time  $\tilde{\tau} > \tau$  one photon is absorbed and the other one remains free. As all Green's functions in this series are retarded, at no point in time can double-excitation of the TLS take place. As a result, the few-photon nonlinearity emerges and induces complex correlations between the photons [38].

## V. PROPERTIES OF THE GREEN'S FUNCTIONS IN THE SINGLE-EXCITATION SECTOR

After having established the diagrammatic formulation of the theory in the single- and double-excitation case, we now turn to the examination of the single-excitation Green's functions and will establish the connection of our framework to the other approaches discussed in Sec. I.

In Sec. II, we have introduced the waveguide as a one-dimensional chain of length  $L$  with nearest-neighbor hopping, thus exhibiting a cosine-shaped dispersion relation  $\epsilon(k) = -2t \cos(k)$ . Although we employ the cosine-shaped dispersion relation in this section, we may also use other dispersion relations (see the discussion in Sec. II). Specifically, we will also consider a linear dispersion relation with group velocity  $v$ , i.e.,  $\epsilon_\mu(k) = \mu vk$ , which is a good approximation for photons in the center of the cosine band. As already indicated in the dispersion relation, we then have to introduce a new quantum number, the chirality  $\mu = R/L = +/-$  in order to account for

the fact that we have both right- and left-moving photons. Furthermore, we pass from a set of discrete sites to a continuum description, which means that we replace all sums over real- or reciprocal space by corresponding integrals and replace  $L$  by  $2\pi$ .

In the continuum limit, Eq. (30) is given by

$$\begin{aligned} {}_1\Sigma(\omega) &= U^2 \int \frac{dk}{2\pi} \frac{1}{\omega + \Omega/2 - \epsilon(k) + i0} \\ &= U^2 \mathcal{P} \int \frac{dk}{2\pi} \frac{1}{\omega + \Omega/2 - \epsilon(k)} \\ &\quad - i\pi U^2 \int \frac{dk}{2\pi} \sum_n \delta(k - k_n) \frac{1}{\partial\epsilon/\partial k} \Big|_{k=k_n}, \end{aligned} \quad (55)$$

where  $\mathcal{P}$  denotes the Cauchy principal value and the  $k_n$  are given by the roots of  $\omega + \Omega/2 = \epsilon(k)$ . If all these roots are real (i.e. the energy is in the band), the principal value in Eq. (55) becomes zero. Moreover, the second term can be identified with the density-of-states of the free waveguide  $\nu(\omega)$ . This gives

$${}_1\Sigma(\omega) = -i\pi U^2 \nu(\omega). \quad (56)$$

As a result, we find that the self-energy for the cosine dispersion as

$${}_1\Sigma_{\cos}(\omega, \Omega) = \frac{U^2}{\omega + \Omega/2 + i\delta - 2t} \sqrt{\frac{\omega + \Omega/2 + i\delta - 2t}{\omega + \Omega/2 + i\delta + 2t}}, \quad (57)$$

and for the linear dispersion as

$${}_1\Sigma_{\text{lin}}(\omega) = -i \frac{U^2}{v}. \quad (58)$$

In the case of linear dispersion, the frequency-independent density-of-states leads to a frequency-independent self-energy. The self-energy of the cosine band exhibits a more complicated structure, it is purely imaginary when  $\omega$  lies inside of the band and purely real when  $\omega$  is outside the band. Note that the given representation of the self-energy is chosen in such a way that the square-root is evaluated at the correct side of the branch cut.

With these two self-energies, we are able to compute the spectral density of the TLS in the single-excitation case as

$${}_1A(\omega) = -\frac{1}{\pi} \text{Im} [{}_1G_e(\omega)]. \quad (59)$$

In Fig. 2, we depict the spectral density for both dispersion relations. The spectral density for the linear dispersion relation is a simple Lorentzian with width  $U^2/v$ . In the case of the cosine dispersion, we clearly observe the frequency span of the band. In addition, we observe two sharp spectral lines in the band gaps on either side of the band that correspond to two atom-photon bound states [19, 26, 39].

Furthermore, knowledge of the Green's functions enables us to compute the scattering matrix ( $S$ -matrix)

$$S_{k,p} = \delta_{k,p} + i2\pi\delta(\epsilon(k) - \epsilon(p))T_{k,p}, \quad (60)$$

where we have obtained the transition matrix ( $T$ -matrix) via the Lehmann-Symanzik-Zimmermann (LSZ) reduction formula [40–42],

$$iT_{k,p} = -iG_0^{-1}(k)G(k,p)G_0^{-1}(p)|_{os}. \quad (61)$$

In this expression,  $G_0(k)$  and  $G(k,p)$  denote, respectively, the free and the full, time-ordered Green's function. Further, the subscript  $os$  indicates that the expression is taken on-shell, i.e., the scattering is elastic (or alternatively  $\omega = \sum_i \epsilon(k_i) = \sum_f \epsilon(k_f)$ , where the sums are over the initial and final momenta, respectively). Using Eqs. (33) and (32) for the free and for the full Green's function, respectively, and omitting the free propagating part yields

$$iT_{k,p} = -i\frac{U^2}{2\pi} {}_1G_e(\omega)|_{os}. \quad (62)$$

We now rewrite the energy-conserving  $\delta$ -function that implements elastic scattering in terms of  $\delta$ -functions with momentum arguments and the density-of-states of the free waveguide

$$\delta(\epsilon(k) - \epsilon(p)) = \pi\nu(\delta_{k,p} + \delta_{k,-p}), \quad (63)$$

Upon combining Eqs. (60) and (62) with Eq. (63) yields

$$S_{k,p} = (1 + r_k)\delta_{k,p} + r_k\delta_{k,-p}, \quad (64)$$

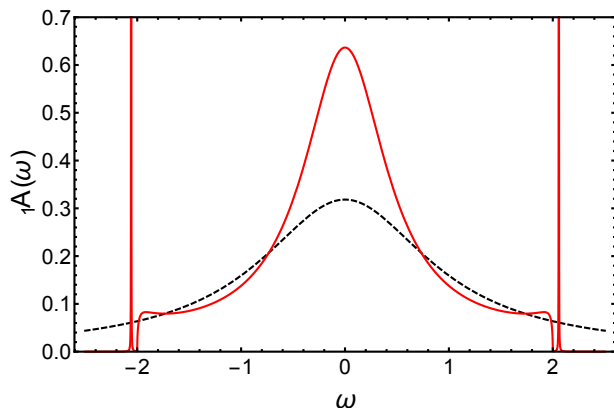


FIG. 2: Spectral density of the TLS with  $\Omega = 0$ ,  $U = 1$ ,  $v = 1$  and  $t = 1$  for the linear (black, dashed) and cosine (red) dispersion relation. The spectral density of the cosine band clearly displays the band edges and features spectrally ultra-sharp bound states in the band gaps on either side of the band (when plotting the spectral density for the cosine band, we have introduced an artificial broadening  $\delta = 10^{-4}$  in order to enhance the visibility of the bound states). By contrast, the spectral density for the linear dispersion relation corresponds to a simple Lorentzian.

where the reflection amplitude  $r_k$  is given by

$$r_k = \frac{-i\pi\nu U^2}{\epsilon(k) - \Omega/2 + i\pi\nu U^2}. \quad (65)$$

In order to compare our results with the results from earlier works [18, 19, 43], we perform a shift of the energy  $\omega \rightarrow \omega - \Omega/2$ . Explicitly, for the linear dispersion relation we obtain

$$r_k^{\text{lin}} = \frac{-iU^2/v}{vk - \Omega + iU^2/v}, \quad (66)$$

while we obtain for the cosine dispersion relation

$$r_k^{\text{cos}} = \frac{-iU^2}{2t|\sin(k)|} \frac{1}{-2t\cos(k) - \Omega + iU^2/2t|\sin(k)|}. \quad (67)$$

Indeed, these expressions are in agreement with the results obtained in earlier works by way of Bethe-Ansatz and LSZ-techniques [18, 19, 43].

## VI. PROPERTIES OF THE GREEN'S FUNCTIONS IN THE TWO-EXCITATION SECTOR

In correspondence with the single-excitation case, we now proceed to analyze the Green's functions in the two-excitation case for the cosine and linear dispersion relations. In addition, we discuss the effect of band edges and bound photon-atom states on the perturbation series.

### A. Cosine dispersion relation - Discrete waveguide

The full Green's function of the TLS is given by Eq. (35) in the form of a perturbation series. This perturbation series can be cast in the form of a  $T$ -Matrix equation, given by Eq. (39). For a discrete waveguide, we can solve this equations simply by (numerical) matrix inversion and we defer the discussion of the continuum limit of the cosine band to sections VIB (band center, approximately linear dispersion) and VIC (band edge, approximately quadratic dispersion).

We define the two-excitation spectral density of the TLS as

$${}_2A(k, \omega) = -\frac{1}{\pi} \text{Im} [{}_2G_e(k, k; \omega)]. \quad (68)$$

In Fig. 3, we depict the two-excitation spectral density of the TLS,  ${}_2A(\pi/2, \omega)$ , and compare with the corresponding single-excitations spectral density,  ${}_1A(\omega)$  (see Fig. 3 for details of the systems). While both spectral densities exhibit an overall similar behavior, we observe an additional feature in the two-excitation spectral density which we attribute to a Fano resonance between the occupied (renormalized) TLS and the additional photon in the waveguide. A Fano resonance appears when a broad

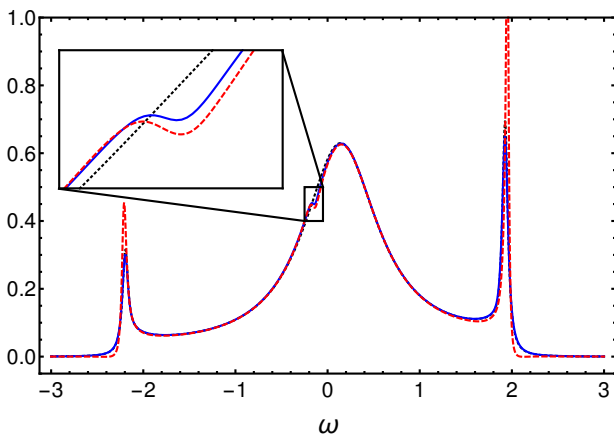


FIG. 3: Single and two-excitation spectral density  ${}_1A(\omega)$  (black dotted) and  ${}_2A(\pi/2, \omega)$  (obtained via the Green's function approach (solid blue) and DMRG (dashed red)) of the TLS with  $\Omega = 0.3$  and  $U = 1$  for a tight-binding waveguide with  $L = 600$  discrete sites and cosine dispersion relation  $\epsilon(k) = -2t \cos(k)$  ( $t = 1$ ). In  ${}_2A(\pi/2, \omega)$ , we clearly observe a Fano-resonance just below  $\omega = 0$  (see text for details). This Fano-resonance is absent in the single-excitation spectral density of the TLS. When plotting the spectral densities, we have introduced an artificial broadening  $\delta = 0.04$  in order to enhance the visibility of the Fano-resonance and to improve numerical convergence.

continuum of states interacts with a single sharp mode. In our case, the (smeared out) TLS plays the role of the continuum whereas the additional photon acts as a sharp resonance. We would like to note that we have introduced an artificial broadening of  $\delta = 0.04$  in order to enhance the visibility of the Fano resonance and to improve numerical convergence of the matrix inversion. As a result, the bound states are not as sharp as in Fig. 2 and the band edges are almost completely smeared out. Therefore, in order to make certain that the broadening does not introduce artificial features, we have confirmed the results of the matrix inversion displayed in Fig. 3 via computations of the spectral density by using an expansion in Chebyshev polynomials within the framework of the Density-Matrix-Renormalization-Group (DMRG) technique as described in [44].

In addition, we would like to stress that a similar Fano-resonance occurs in (analytically solvable) case of linear dispersion (see Sec. VI B) so that we conclude that the occurrence of such a Fano-resonance between the occupied (renormalized) TLS and the additional photon in the waveguide is a generic feature of the few-photon non-linearity in the  $n$ -photon-transport through a waveguide with embedded TLS for  $n > 1$ .

Although we have solved Eq. (39) for a cosine dispersion relation only, we would like to stress that our formalism is certainly not limited to this case (see the discussion in section II). In fact, the  $T$ -matrix equation (39) is applicable to every possible dispersion relation that can be

realized in a one-dimensional waveguide.

## B. Linear dispersion relation

We now turn to our attention to the case of an (infinitely extended) linear dispersion relation  $\epsilon_\mu(k) = \mu vk$  and thus ignore the effects of band edges, notably bound photon-atom states and slow light regimes. Just as in the single-excitation case, we transit to the continuum limit. Then, the self-energy of the renormalized TLS-Green's functions is

$${}_2\Sigma_{\text{lin}}(k; \omega) = -i \frac{U^2}{v}, \quad (69)$$

i.e., the same expression as in the single-excitation sector. This suggests that the linear dispersion exhibits certain special features so that, in contrast to the numerical treatment of the  $T$ -matrix, we aim at directly summing up the perturbation series, Eq. (35). Formally, we can rewrite this series as

$${}_2G_e(k_f, k_i; \omega) = \sum_i {}_2G_e^{(i)}(k_f, k_i; \omega). \quad (70)$$

Clearly, the first two terms of the series can be written down immediately, as no integration over internal momenta is required.

The third term, however, is given by

$$\begin{aligned} & {}_2G_e^{(3)}(k_f, k_i; \omega) \\ &= \frac{U^4}{2\pi} \int \frac{dk}{2\pi} {}_2G_{e,r}(k_i; \omega) {}_2G_w^0(k_i, k; \omega) \\ & \quad \times {}_2G_{e,r}(k; \omega) {}_2G_w^0(k, k_f; \omega) \\ & \quad \times {}_2G_{e,r}(k_f; \omega), \end{aligned} \quad (71)$$

where the integral only extends over the three internal Green's functions. As all these Green's functions have single poles that are shifted into the upper half plane, it follows that the integral and hence the entire third term in the series vanishes. As a matter of fact, this argument can be applied to terms of order higher or equal to three and this means that, in the case of a linear dispersion, the full TLS-Green's function is completely determined by the first two terms

$$\begin{aligned} & {}_2G_e(k_f, k_i; \omega) \\ &= {}_2G_{e,r}(k_i; \omega) \delta_{k_i, k_f} \\ & \quad + \frac{U^2}{2\pi} {}_2G_{e,r}(k_i; \omega) {}_2G_w^0(k_f, k_i; \omega) {}_2G_{e,r}(k_f; \omega). \end{aligned} \quad (72)$$

We are now in a position to provide a physical explanation for this termination of the perturbation series for linear dispersion relations after the first two terms by inspecting the first vanishing Feynman diagram (i.e., the third diagram on the r.h.s. of Eq. (54)) in the time domain

$${}_2G_e^{(3)}(k_f, k_i; \omega) = \begin{array}{c} \text{---} \circledast \text{---} \\ \text{---} \circledast \text{---} \\ \text{---} \circledast \text{---} \end{array} \quad (73)$$

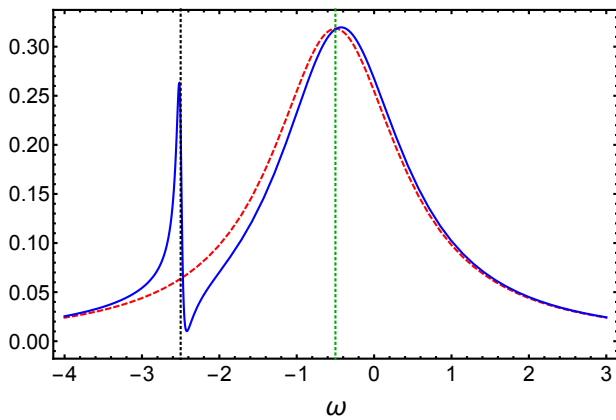


FIG. 4: Single- and two-excitation spectral densities  ${}_2A(-1, \omega)$  (solid blue) and  ${}_1A(\omega)$  (dashed red) of the TLS with  $\Omega = 1$  and  $U = 1$  for a waveguide with linear dispersion relation  $\epsilon(k) = \mu vk$  and  $v = 1$  considered in the continuum limit. We have shifted the single-excitation spectral density  ${}_1A(\omega)$  by  $\omega \rightarrow \omega - vk$ , so that the maxima of both plots overlap. The green dotted line is at  $vk + \Omega/2$  and indicates the maximum of  ${}_1A(\omega)$ . In  ${}_2A(-1, \omega)$ , we clearly observe a Fano-resonance at  $\omega = 2vk - \Omega/2$  (black-dotted line) which is more pronounced than for the case of tight-binding waveguide in Fig. 3. As in the case of the tight-binding waveguide, this Fano-resonance is absent in the single-excitation spectral density of the TLS. When plotting the spectral densities, we have introduced the same artificial broadening  $\delta = 0.04$  as in the case of the tight-binding waveguide in order to enhance the visibility of the Fano-resonance and make the graph comparable to that in Fig. 3.

The particle of interest is the (intermediary) upper photon, which is emitted and reabsorbed by the TLS. During the time that the upper photon "lives", the initial photon propagates and eventually gets absorbed. After a while, the photon is re-emitted and propagates further for a certain time. The entire process occupies a certain time  $\tau > 0$ . During this time, the upper (intermediate) photon moves a certain distance due to the fixed group velocity  $v > 0$  of the linear dispersion and the absence of back-scattering mechanisms. This means that the photon has moved away from the TLS and actually cannot be re-absorbed, hence the diagram vanishes. We would like to note that this is a special property of the linear dispersion relation and does not hold for general dispersions relations, notably not near band edges and/or waveguide cut-off frequencies, i.e., in the vicinity of slow-light regimes.

We have calculated the two-excitation spectral density according to Eq. (68) and depict the results together with the single-excitation spectral density in Fig. 4. Similar to the numerical calculations for the cosine dispersion relation we, again, find again a Fano resonance located at  $\omega_F = 2vk - \Omega/2$ , which, however, is much more pronounced than in the cosine-shaped dispersion case. Comparing both dispersion relations, the Fano resonance ap-

pears in two different ways: In the case of the cosine dispersion relation the Fano resonance emerges as a result of the self-consistent treatment of the T-Matrix, whereas for the linear dispersion relation it can be traced back to the second term in the perturbation series  ${}_2G_e^{(2)}(k_f, k_i; \omega)$ . To be more exact, the Fano resonance stems from the internal free waveguide Green's function  ${}_2G_w^0(k_i, k_f; \omega)$ , which is of the form  $(\omega - \omega_F + i\delta)^{-1}$ . As a result, the Fano resonance is the consequence of a first order pole, regularized by a finite imaginary factor  $i\delta$ . For sufficiently small  $\delta$ , the spectral density can thus even assume negative values. However, one has to take into account that we are not considering the spectral density of the full system, but only of a part of it (i.e., the part stemming from the TLS). Therefore, a negative spectral density is acceptable and can be considered as some sort of "gain" (where the energy is taken from the waveguide), indicating effects such as photon bunching [18, 38, 45]. Moreover, we would like to point out that the Fano resonance is less pronounced in Fig. 3, although all energies (transition energy of the TLS, photon energy) are in the linear regime of the cosine band. We attribute this regularization to the self-consistent treatment of the Green's function, which is not possible for the linear dispersion relation.

In fact, the deeper reason behind the termination of the perturbation series for the linear dispersion is the separation of the photons on the Hamiltonian level into two kinds of photons (left- and right-moving ones). This changes the symmetry of the original Hamiltonian, i.e., the chirality is introduced as a new quantum number, and eventually leads to the special analytic structure of the Green's functions and, as a consequence, to the termination of the perturbation series.

Finally, we can now construct the two-excitation  $S$ -matrix by generalizing the LSZ formalism presented in Sec. V. Explicitly, the two-excitation  $S$ -Matrix is given as

$$S_{k_i p_i, k_f p_f} = (\delta_{k_i, k_f} \delta_{p_i, p_f} + \delta_{p_i, k_f} \delta_{k_i, p_f}) + i2\pi\delta(E) T_{k_i p_i, k_f p_f}, \quad (74)$$

where

$$\delta(E) = \delta(\epsilon(k_i) + \epsilon(p_i) - \epsilon(k_f) - \epsilon(p_f)) \quad (75)$$

ensures elastic scattering and the associated  $T$ -matrix is defined as

$$iT_{k_i p_i, k_f p_f} = -iG_0^{-1}(k_i, p_i) G(k_i, p_i; k_f, p_f) G_0^{-1}(k_f, p_f)|_{os}. \quad (76)$$

In this expression,  $G_0(k, p)$  and  $G(k, p; k', p')$  denote, respectively, the free and the full waveguide Green's function. With the help of Eq. (42), we explicitly find

$$iT_{k_i p_i, k_f p_f} = -i\frac{U^2}{2\pi} {}_2G_e^{\text{sym}}(k_i, p_i, k_f, p_f; \omega)|_{os}, \quad (77)$$

where  ${}_2G_e^{\text{sym}}(k_i, p_i, k_f, p_f; \omega)$  is defined by Eq. (43).

In order to compare these results with results of earlier works, we again perform a frequency shift  $\omega \rightarrow \omega - \Omega/2$ . We carry out the actual calculations of the  $S$ -Matrix in Appendix D so that we report here only the final results. For different chirality configurations, the  $S$ -matrix reads

- $k_i^R p_i^R \rightarrow k_f^R p_f^R$ 

$$S_{k_i p_i, k_f p_f}^{RR, RR} = t_{k_i} t_{p_i} (\delta_{k_i, k_f} \delta_{p_i, p_f} + \delta_{k_i, p_f} \delta_{p_i, k_f}) + S_{k_i p_i, k_f p_f}^{2, P.V.}, \quad (78)$$

- $k_i^R p_i^R \rightarrow k_f^R p_f^L$ 

$$S_{k_i p_i, k_f p_f}^{RR, RL} = t_{k_i} r_{p_i} \delta_{k_i, k_f} \delta_{p_i, -p_f} + r_{k_i} t_{p_i} \delta_{k_i, -p_f} \delta_{p_i, k_f} + S_{k_i p_i, k_f p_f}^{2, P.V.}, \quad (79)$$

- $k_i^R p_i^R \rightarrow k_f^L p_f^L$ 

$$S_{k_i p_i, k_f p_f}^{RR, LL} = r_{k_i} r_{p_i} (\delta_{k_i, -k_f} \delta_{p_i, -p_f} + \delta_{k_i, -p_f} \delta_{p_i, -k_f}) + S_{k_i p_i, k_f p_f}^{2, P.V.}, \quad (80)$$

In these expressions, the superscript of the momenta indicates the chirality,  $r_k$  is the single-excitation reflection amplitude (c.f. Eq. (66)),  $t_k = 1 + r_k$  is the single-excitation transmission amplitude and  $S_{k_i p_i, k_f p_f}^{2, P.V.}$  is given by

$$S_{k_i p_i, k_f p_f}^{2, P.V.} = \frac{iU^4}{\pi v} \delta_{k_i + p_i, k_f + p_f} \times \frac{(k_i + p_i - 2\Omega + iU^2/v)}{(vp_i - \Omega + iU^2/v)(vk_i - \Omega + iU^2/v)} \times \frac{1}{(vp_f - \Omega + iU^2/v)(vk_f - \Omega + iU^2/v)}. \quad (81)$$

Our results are thus in accordance with the results obtained by other techniques in earlier works [18, 19, 45].

Within our scheme, we can also give a new explanation of the term  $S_{k_i p_i, k_f p_f}^{2, P.V.}$ . In the first place, this term appears by replacing the free waveguide-Green's function in  ${}_2G_e^{(2)}$  by the Dirac identity

$$\frac{1}{\omega - vk - vp + i0} = \mathcal{P} \frac{1}{\omega - vk - vp} - i\pi \delta(\omega - vk - vp). \quad (82)$$

The two terms in the Dirac identity can be interpreted as follows. The imaginary part that is proportional to a  $\delta$ -function corresponds to long-time, real processes, because the  $\delta$ -function sets the particles on-shell. The real part that contains the principal value, however, does not place a constraint on the momenta. The momenta can be chosen freely and are only restricted by energy conservation. Therefore, this term corresponds to short times, which are on the scale of the Heisenberg uncertainty principle, i.e., they correspond to *virtual processes*.

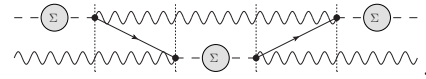
### C. Band edge effects

Finally, we address the case of band edges by following the same line of reasoning as in section VI B. Perhaps the simplest nonlinear dispersion relations exhibiting a band edge is the quadratic dispersion relations  $\epsilon(k) = tk^2$  with  $t > 0$ . In this case, the self-energy is given by

$${}_2\Sigma_{\text{qu}}(k; \omega) = -i \frac{\pi U^2}{\sqrt{t(\omega - tk^2 + i0)}}, \quad (83)$$

where we scaled out the factor  $\Omega/2$  again. The first two terms of the perturbation series given by Eq. (70) can again be computed straightforwardly, but the third term (and all higher-order terms) exhibit different characteristics. First of all, the quadratic dispersion relation induces poles on both sides of the complex half-plane, which means that the integral over internal momenta is not vanishing, hence  ${}_2G_e^{(3)}(k_f, k_i; \omega)$  is finite. This was expected, since the quadratic dispersion relation exhibits a state where the group velocity  $v_g = 0$ , which means that an emitted photon can be reabsorbed by the TLS after a certain amount of time (c.f. discussion in section VI B). Secondly, the self-energy  ${}_2\Sigma_{\text{qu}}(k; \omega)$  leads to two branch cuts, one in each half space of the complex plane. These branch cuts represent major obstacles in the integration over the internal momenta and we have been unable to find a closed form-solution for  ${}_2G_e^{(3)}(k_f, k_i; \omega)$ .

From a more physical point of view, however, we expect that the higher-order processes encapsulate the effect of interaction-induced radiation trapping (IIRT) [26, 39]. This phenomenon describes the excitation of the atom-photon bound state by a two-photon pulse as the result of a nonlinear process. This expectation can be motivated by the diagrammatic form of  ${}_2G_e^{(3)}(k_f, k_i; \omega)$ ,



In the top line the TLS emits a photon, which is reabsorbed at a later time. This is exactly the behavior one would expect from the atom-photon bound state, since the radiation cannot leave the TLS.

The prototypical process of IIRT includes two initial photons, which are transformed into an atom-photon bound state and a photon with a different momentum. Energetically, this process is described by

$$\omega = \epsilon(k_i) + \epsilon(p_i) = \omega_{\text{BS}} + \epsilon(k_f), \quad (84)$$

where  $k_i$  and  $p_i$  are the momenta of the initial photons,  $k_f$  is the momentum of the final photon,  $\omega$  is the total energy and  $\omega_{\text{BS}}$  is the energy of the bound atom-photon state, which can be found by solving the equation

$$\omega_{\text{BS}} - \Omega + i \frac{U^2 \pi}{\sqrt{t\omega_{\text{BS}}}} = 0. \quad (85)$$

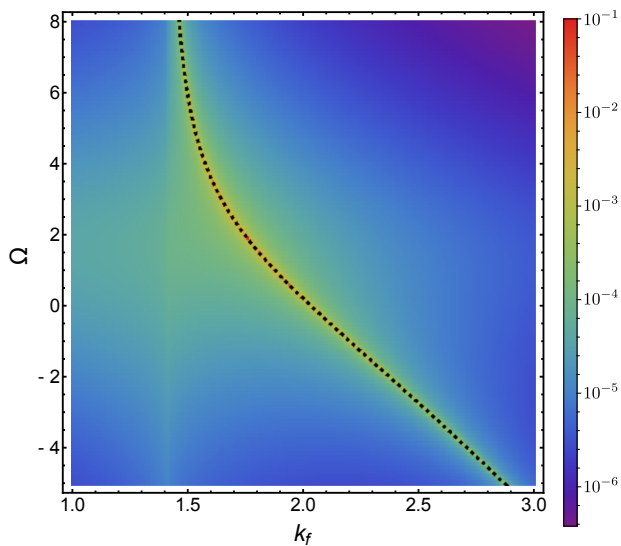


FIG. 5: Logarithmic plot of  $|{}_2G_e^{(3)}(k_f, k_i; \omega)|$  with  $k_i = p_i = 1$ ,  $t = 1$ ,  $U = 1$ ,  $\omega = \epsilon(k_1) + \epsilon(k_2)$ . We have added a small imaginary part  $\delta = 10^{-3}$  to  $\omega$  for an artificial broadening of the resonance. The black dotted line represents the solution of  $\omega = \omega_{BS} + \epsilon(k_f)$ . The resonance approaches  $k_f \rightarrow \sqrt{2}$  for large values of  $\Omega$ , since the bound state energy  $\omega_{BS} \rightarrow 0$  in this case.

In fact, setting  ${}_2G_e^{(3)}(k_f, k_i; \omega)$  on-shell (thus making it proportional to a scattering matrix element) and computing the integration over the internal momenta numerically yields a sharp peak at precisely the momenta  $k_f$  which fulfill  $\omega = \omega_{BS} + \epsilon(k_f)$  (cf. Fig. 5). This indicates that  ${}_2G_e^{(3)}(k_f, k_i; \omega)$  (together with the higher-order processes) describes indeed the physics behind the IIRT. Moreover, treating the sharp peak as a pole (which is motivated by the fact that the width of the resonance scales with the small imaginary part  $i\delta$ ) enables us to compute the residue of the resonance via

$$\text{Res} [{}_2G_e^{(3)}, k_0] = \frac{1}{2\pi i} \oint_C dz {}_2G_e^{(3)}(z, k_i; \omega)|_{os}, \quad (86)$$

where  $k_0$  is the solution of Eq. (84), the subscript *os* indicates that the expression is taken on-shell and the contour  $C$  is a circle centered at  $k_0$  with radius  $\eta$ . We have plotted the residue in Fig. 6, together with the conditions that the two initial photons are on resonance with the TLS individually ( $\Omega = \epsilon(k_i)$ ) and collectively ( $\Omega = \omega = 2\epsilon(k_i)$ ). We can see here that the strength of the pole is sensitive to the TLS being on resonance with the collective photonic excitation, rather than with the individual ones. This is another indicator that IIRT emerges as the result of the nonlinear behavior of the TLS in the presence of two or more photons. Furthermore, this result shows that an analytic solution for  ${}_2G_e^{(3)}(k_f, k_i; \omega)$  is still highly desirable as this would provide further insights into the physics of IIRT.

Finally, we would like to conclude this section by recalling the physical interpretation of each term in the

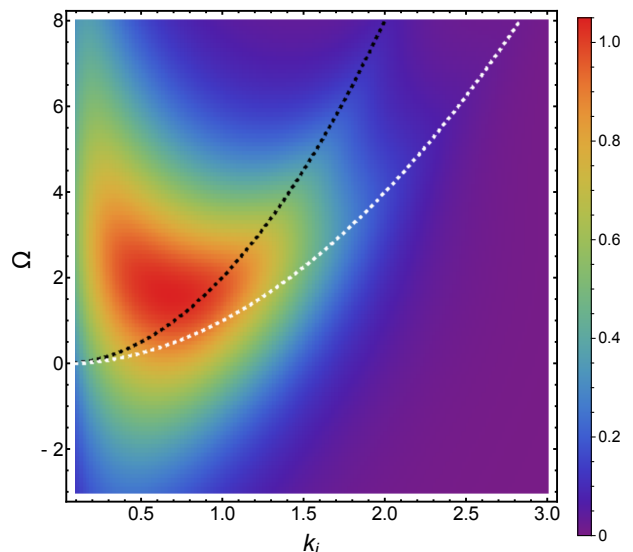


FIG. 6: Plot of  $|\text{Res} [{}_2G_e^{(3)}, k_0]|$  for two identical initial photons  $\omega = 2\epsilon(k_i)$ ,  $U = 1$ ,  $t = 1$ ,  $\delta = 10^{-4}$  and  $\eta = 10^{-6}$ . The black and white lines represent the parabolas  $\Omega = 2\epsilon(k_i)$  and  $\Omega = \epsilon(k_i)$ , respectively.

perturbation series of  ${}_2G_e(k_f, k_i; \omega)$ : The first term describes the single-photon scattering and does not induce correlations between the two photons. The second term gives rise to photon bunching and is always finite, independent of the dispersion relation. The third term and all higher-order terms are nontrivial, since they include integrations over internal momenta. In the case of a linear dispersion relation their contribution vanishes. Conversely, these higher-order terms become particularly relevant for frequencies near band edges and/or waveguide cut-offs and lead to the effect of IIRT.

## VII. CONCLUSION

In summary, we have developed an efficient and flexible quantum field theoretical approach to few-photon transport problems in one-dimensional photonic waveguides with embedded quantum impurities. Our approach is based on a coherent-state path integral formulation which allows us to formulate a Feynman diagram representation that elucidates the nature of the underlying physical processes. For instance, our framework allows for both frequency- and time-domain considerations and we have utilized both of them throughout this manuscript in order to arrive at several novel physical explanations.

In the case of a single excitation, our approach delivers closed-form analytical expressions for the Green's functions for arbitrary dispersion relations and we have computed spectral densities and scattering matrices. Similarly, for the case of two excitations, our approach demonstrates that and why all diagrams of order higher than







In order to calculate  $S_{k_i p_i, k_f p_f}^1$ , we rewrite the  $\delta$ -function according to

$$\delta(\epsilon(k_i) + \epsilon(p_i) - \epsilon(k_f) - \epsilon(p_f)) = \frac{\delta_{k_i + p_i, k_f + p_f}}{v}. \quad (\text{D5})$$

Bearing in mind that we have shifted  $\omega \rightarrow \omega - \Omega/2$ , using Eq. (37), and setting  $\omega = vk_i + vp_i$ , we find after cumbersome but straightforward calculation

$$\begin{aligned} S_{k_i p_i, k_f p_f}^1 &= \delta_{p_i, p_f} \delta_{k_i, k_f} \frac{-iU^2/v}{vp_i - \Omega + iU^2/v} + \{\text{perm}\} \\ &= r_{k_i} (\delta_{p_i, p_f} \delta_{k_i, k_f} + \delta_{p_i, k_f} \delta_{k_i, p_f}) \\ &\quad + r_{p_i} (\delta_{p_i, p_f} \delta_{k_i, k_f} + \delta_{p_i, k_f} \delta_{k_i, p_f}). \end{aligned} \quad (\text{D6})$$

Here,  $r_k$  is the single-excitation reflection amplitude as specified in Eq. (66).

In very much the same manner, we find

$$\begin{aligned} S_{k_i p_i, k_f p_f}^2 &= \delta_{k_i + p_i, k_f + p_f} \frac{-iU^4}{2\pi v} \frac{1}{vk_i - \Omega + iU^2/v} \\ &\quad \times \frac{1}{vk_f - vp_i + i0} \frac{1}{vp_f - \Omega + iU^2/v} + \{\text{perm}\}. \end{aligned} \quad (\text{D7})$$

Upon replacing the inner free Green's function by an application of the Dirac identity

$$\frac{1}{x + i0} = \mathcal{P} \left( \frac{1}{x} \right) - i\pi \delta(x), \quad (\text{D8})$$

the scattering matrix decomposes into two terms

$$S_{k_i p_i, k_f p_f}^2 = S_{k_i p_i, k_f p_f}^{2, \text{P.V.}} + S_{k_i p_i, k_f p_f}^{2, \delta}, \quad (\text{D9})$$

where the term that results from the  $\delta$ -function in the Dirac identity,  $S_{k_i p_i, k_f p_f}^{2, \delta}$ , reduces to

$$\begin{aligned} S_{k_i p_i, k_f p_f}^{2, \delta} &= \frac{1}{2} \delta_{p_i, p_f} \delta_{k_i, k_f} \frac{-iU^2/v}{vk_i - \Omega + iU^2/v} \\ &\quad \times \frac{-iU^2/v}{vp_f - \Omega + iU^2/v} + \{\text{perm}\} \\ &= r_{k_i} r_{p_i} (\delta_{p_1, p_2} \delta_{k_1, k_2} + \delta_{k_1, p_2} \delta_{p_1, k_2}). \end{aligned} \quad (\text{D10})$$

The term of the scattering matrix that originates from the principal value in the Dirac identity is given by

$$\begin{aligned} S_{k_i p_i, k_f p_f}^{2, \text{P.V.}} &= \frac{i}{2\pi} \delta_{k_i + p_i, k_f + p_f} r_{k_i} r_{p_f} \mathcal{P} \frac{1}{k_i - k_f} + \{\text{perm}\} \\ &= \frac{i}{2\pi} \delta_{k_i + p_i, k_f + p_f} \left[ \mathcal{P} \frac{1}{k_i - k_f} (r_{k_i} r_{p_f} - r_{p_i} r_{k_f}) \right. \\ &\quad \left. + \mathcal{P} \frac{1}{k_i - p_f} (r_{k_i} r_{k_f} - r_{p_i} r_{p_f}) \right]. \end{aligned} \quad (\text{D11})$$

Here, we have used energy conservation to facilitate certain simplifications. Using energy conservation another

time, we find

$$\begin{aligned} r_{k_i} r_{p_f} - r_{p_i} r_{k_f} &= \frac{U^4}{v} \frac{(k_i - k_f) (E - 2\Omega + iU^2/v)}{(vp_i - \Omega + iU^2/v)(vk_i - \Omega + iU^2/v)} \\ &\quad \times \frac{1}{(vp_f - \Omega + iU^2/v)(vk_f - \Omega + iU^2/v)} \end{aligned} \quad (\text{D12})$$

and the same expression with interchanged momenta,  $k_f \leftrightarrow p_f$ , for  $r_{k_i} r_{k_f} - r_{p_i} r_{p_f}$ . Exploiting the fact that

$$(k_i - k_f) \mathcal{P} \frac{1}{k_i - k_f} = 1 \quad (\text{D13})$$

and combining the above expressions, we find

$$\begin{aligned} S_{k_i p_i, k_f p_f}^{2, \text{P.V.}} &= \frac{iU^4}{\pi v} \delta_{k_i + p_i, k_f + p_f} \\ &\quad \times \frac{(k_i + p_i - 2\Omega + iU^2/v)}{(vp_i - \Omega + iU^2/v)(vk_i - \Omega + iU^2/v)} \\ &\quad \times \frac{1}{(vp_f - \Omega + iU^2/v)(vk_f - \Omega + iU^2/v)}. \end{aligned} \quad (\text{D14})$$

Upon inserting Eq. (D2), (D6), and (D10) in (D1), we finally find

$$\begin{aligned} S_{k_i p_i, k_f p_f}^{RR, RR} &= t_{k_i} t_{p_i} (\delta_{k_i, k_f} \delta_{p_i, p_f} + \delta_{k_i, p_f} \delta_{p_i, k_f}) \\ &\quad + S_{k_i p_i, k_f p_f}^{2, \text{P.V.}}, \end{aligned} \quad (\text{D15})$$

where  $t_k = 1 + r_k$ . As a matter of fact, the above expression is exactly the scattering matrix given in Ref. 18.

We now turn to the effects of chirality. First, the momenta are renormalized  $k \rightarrow \mu k$ , which controls the sign of the momenta. Second, chirality is conserved upon free propagation, which adds two chirality conserving  $\delta$ -functions to  $S_{k_i p_i, k_f p_f}^0$  and one to  $S_{k_i p_i, k_f p_f}^1$ . Combining all the relevant expressions, the  $S$ -matrix in the other chirality sectors calculates to

$$\begin{aligned} \bullet k_i^R p_i^R &\rightarrow k_i^R p_f^L \\ S_{k_i p_i, k_f p_f}^{RR, RL} &= t_{k_i} r_{p_i} \delta_{k_i, k_f} \delta_{p_i, -p_f} + r_{k_i} t_{p_i} \delta_{k_i, -p_f} \delta_{p_i, k_f} \\ &\quad + S_{k_i p_i, k_f p_f}^{2, \text{P.V.}}, \end{aligned} \quad (\text{D16})$$

$$\begin{aligned} \bullet k_i^R p_i^R &\rightarrow k_f^L p_f^L \\ S_{k_i p_i, k_f p_f}^{RR, LL} &= r_{k_i} r_{p_i} (\delta_{k_i, -k_f} \delta_{p_i, -p_f} + \delta_{k_i, -p_f} \delta_{p_i, -k_f}) \\ &\quad + S_{k_i p_i, k_f p_f}^{2, \text{P.V.}}, \end{aligned} \quad (\text{D17})$$

where the superscripts of  $k_j^\mu$  indicate the values of chirality.

- 
- [1] J. L. O'Brien, A. Furusawa, and J. Vučković, *Nature Photonics* **3**, 687 (2009).
- [2] O. Benson, *Nature* **480**, 193 (2011).
- [3] A. W. Schell, J. Kaschke, J. Fischer, R. Henze, J. Wolters, M. Wegener, and B. O., *Scientific Reports* **3**, 1577 (2013).
- [4] J. Q. You and F. Nori, *Nature* **474**, 589 (2011).
- [5] M. H. Devoret and J. R. Schoelkopf, *Science* **339**, 1169 (2013).
- [6] R. Mitsch, C. Sayrin, B. Albrecht, P. Schneeweiss, and A. Rauschenbeutel, *Nature Communications* **5**, 5713 (2014).
- [7] A. J. Shields, *Nature Photonics* **1**, 215 (2007).
- [8] J. Claudon, J. Bleuse, N. S. Malik, M. Bazin, P. Jaffrennou, N. Gregersen, C. Sauvan, P. Lalanne, and J.-M. Gerard, *Nature Photonics* **4**, 174 (2010).
- [9] A. Laucht, S. Pütz, T. Günthner, N. Hauke, R. Saive, S. Frédérick, M. Bichler, M.-C. Amann, A. W. Holleitner, M. Kaniber, et al., *Phys. Rev. X* **2**, 011014 (2012).
- [10] S. Fattahpoor, T. B. Hoang, L. Midolo, C. P. Dietrich, L. H. Li, E. H. Linfield, J. F. P. Schouwenberg, T. Xia, F. M. Pagliano, F. M. W. van Otten, et al., *Appl. Phys. Lett.* **102**, 131105 (2013).
- [11] R. H. Hadfield, *Nature Photonics* **3**, 696 (2009).
- [12] W. H. P. Pernice, C. Schuck, O. Minaeva, M. Li, G. N. Goltsman, A. V. Sergienko, and H. X. Tang, *Nature Communications* **3**, 1325 (2012).
- [13] D. Sahin, A. Gaggero, Z. Zhou, S. Jahanmirinejad, F. Mattioli, R. Leoni, J. Beetz, M. Lerner, M. Kamp, S. Höfling, et al., *Appl. Phys. Lett.* **103**, 111116 (2013).
- [14] F. Najafi, J. Mowver, N. C. Harris, F. Bellei, A. Dane, C. Lee, X. Hu, P. Kharel, F. Marsili, S. Assefa, et al., *Nature Communications* **6**, 5873 (2015).
- [15] D. E. Chang, V. Vuletić, and M. D. Lukin, *Nature Photonics* **8**, 685 (2014).
- [16] J. Volz, M. Scheucher, C. Junge, and A. Rauschenbeutel, *Nature Photonics* **8**, 965 (2014).
- [17] P. Lodahl, S. Mahmoodian, and S. Stobbe, *Rev. Mod. Phys.* **87**, 347 (2015).
- [18] J.-T. Shen and S. Fan, *Phys. Rev. A* **76**, 062709 (2007).
- [19] T. Shi and C. P. Sun, *Phys. Rev. B* **79**, 205111 (2009).
- [20] S. Fan, S. E. Kocabas, and J.-T. Shen, *Phys. Rev. A* **82**, 063821 (2010).
- [21] M. Pletyukhov and V. Gritsev, *New Journal of Physics* **14**, 095028 (2012).
- [22] H. Zheng, D. J. Gauthier, and H. U. Baranger, *Phys. Rev. A* **82**, 063816 (2010).
- [23] H. Zheng, D. J. Gauthier, and H. U. Baranger, *Phys. Rev. Lett.* **107**, 223601 (2011).
- [24] H. Zheng, D. J. Gauthier, and H. U. Baranger, *Phys. Rev. A* **85**, 043832 (2012).
- [25] P. Longo, P. Schmitteckert, and K. Busch, *J. Opt. A* **11**, 114009 (2009).
- [26] P. Longo, P. Schmitteckert, and K. Busch, *Phys. Rev. Lett.* **104**, 023602 (2010).
- [27] A. Nysteen, D. P. S. McCutcheon, and J. Mørk, *New J. Phys.* **17**, 023030 (2015).
- [28] E. Sanchez-Burillo, D. Zueco, J. J. Garcia-Ripoll, and L. Martin-Moreno, *Phys. Rev. Lett.* **113**, 263604 (2014).
- [29] M. Notomi, E. Kuramochi, and T. Tanabe, *Nat. Photon.* **2**, 741 (2008).
- [30] H. Takesue, N. Matsuda, E. Kuramochi, W. J. Munro, and M. Notomi, *Nat. Commun.* **4**, 2725 (2013).
- [31] A. W. Schell, H. Takashima, S. Kamioka, Y. Oe, M. Fujiwara, B. O., and S. Takeuchi, *Scientific Reports* **5**, 9619 (2015).
- [32] E. Jaynes and F. W. Cummings, *Proceedings of the IEEE* **51**, 89 (1963), ISSN 0018-9219.
- [33] R. Dicke, *Phys. Rev.* **93**, 99 (1954).
- [34] P. W. Anderson, *Phys. Rev.* **124**, 41 (1961).
- [35] J. Rammer, *Quantum Transport Theory*, *Frontiers in Physics Series* (Westview Press, 2004), ISBN 9780813346229.
- [36] J. Rammer, *Quantum Field Theory of Non-equilibrium States* (Cambridge University Press, 2007), ISBN 9781139465014.
- [37] T. Boudjedaa, A. Bounames, K. Nouicer, L. Chetouani, and T. F. Hammann, *Physica Scripta* **54**, 225 (1996).
- [38] M. Moederdt, P. Schmitteckert, and K. Busch, *Opt. Lett.* **38**, 3693 (2013).
- [39] P. Longo, P. Schmitteckert, and K. Busch, *Phys. Rev. A* **83**, 063828 (2011).
- [40] H. Lehmann, K. Symanzik, and W. Zimmermann, *Il Nuovo Cimento* **1**, 205 (1955), ISSN 0029-6341.
- [41] G. Zaránd, L. Borda, J. von Delft, and N. Andrei, *Phys. Rev. Lett.* **93**, 107204 (2004).
- [42] L. Borda, L. Fritz, N. Andrei, and G. Zaránd, *Phys. Rev. B* **75**, 235112 (2007).
- [43] L. Zhou, Z. R. Gong, Y.-x. Liu, C. P. Sun, and F. Nori, *Phys. Rev. Lett.* **101**, 100501 (2008).
- [44] A. Braun and P. Schmitteckert, *Phys. Rev. B* **90**, 165112 (2014).
- [45] J.-T. Shen and S. Fan, *Phys. Rev. Lett.* **98**, 153003 (2007).
- [46] G. Mahan, *Many-Particle Physics*, *Physics of Solids and Liquids* (Springer, 2000), ISBN 9780306463389.